Article:
Zeng, H, Konicek, AR, Moldovan, N et al. (7 more authors) (2015) Boron-doped ultrananocrystalline diamond synthesized with an H-rich/Ar-lean gas system. Carbon, 84. pp. 103-117. ISSN 0008-6223

https://doi.org/10.1016/j.carbon.2014.11.057

Boron-Doped Ultrananocrystalline Diamond Synthesized with an H-Rich/Ar-Free Gas System

Hongjun Zeng*[1], Andrew R. Konicek[2, †], Nicolaie Moldovan[1], Filippo Mangolini[2], Tevis Jacobs[2], Ian Wylie[1], Prabhu U. Arumugam[1, $], Shabnam Siddiqui[1], Robert W. Carpick[3], John A. Carlisle[1]

1. Advanced Diamond Technologies, Inc., Romeoville, IL 60565
2. Department of Materials Science and Engineering, University of Pennsylvania, Philadelphia, PA 19104
3. Department of Mechanical Engineering and Applied Mechanics, University of Pennsylvania, Philadelphia, PA 19104

† Present address: Corporate Strategic Research, ExxonMobil Research and Engineering, Annandale, NJ

$ Present address: : Institute for Micromanufacturing, Louisiana Tech University, Ruston LA 71272

* Corresponding author. Tel: 815 293-0900. E-mail: zeng@thindiamond.com (H. Zeng).

Abstract: This paper reports the recent development and applications of conductive boron-doped ultrananocrystalline diamond (BD-UNCD). The authors have determined that BD-UNCD can be synthesized with an H-rich gaseous chemistry and a high CH_4/H_2 ratio, which is opposite to previously reported methods with Ar-rich or H-rich gas compositions but utilizing very low CH_4/H_2 ratio. The BD-UNCD has a resistivity as low as 0.01 ohm·cm, with low roughness (down to several nm) and a wide deposition temperature range (450-850ºC). The properties of this BD-UNCD were studied systematically using resistivity characterization, scanning electron microscopy, transmission electron microscopy, Raman spectroscopy, and roughness measurements. Near Edge X-ray Absorption Fine Structure (NEXAFS) spectroscopy confirms that up to 97% of the UNCD is deposited as sp3 carbon. These series of measurements also reveal additional unique properties for this material, such as an "M" shape Raman signature, line-granular nano-cluster texture and high C-H bond surface content. A hypothesis is provided to explain why this new deposition strategy, with H-rich/Ar-free gas chemistry and CH_4/H_2 ratio, is able to produce high sp3-content and/or

heavily doped UNCD. In addition, a few emerging applications for BD-UNCD in the field of atomic force microscopy, electrochemistry and biosensing are reviewed here.

1. Introduction

Ultrananocrystalline diamond (UNCD) is the newest member of diamond family, and it has attracted significant interests over the last two decades. [1-3] While maintaining most of the exceptional physical/chemical properties of conventional diamond materials, UNCD has an extremely low grain size (3-5 nm) and roughness (sub-10 nm) independent of thickness, which drives its popularity as an engineering and functional martial, especially in the fields of tribology, biology, and micro/nano-technology. [4-5] In conventional polycrystalline diamond coatings, for either nanocrystalline diamond (NCD) or microcrystalline diamond (MCD), the gas composition usually consists of CH_4 or other carbon source with majority of hydrogen gas in a chemical vapor deposition (CVD) reactor. However, in the prior art, UNCD is only synthesized with an Ar-rich/H-lean gas chemistry. Gruen *et al* explained that the role of Ar is primarily to assist in the generation of a large number of C_2 dimer molecules which act as the principal growth species for UNCD. These C2 dimers also acts as renucleation species which contribute to the high renucleation rate for UNCD and the resulting small grain size of UNCD. [4, 6] In this report, we show that Ar-rich gas mixtures are not the only gas system able to produce UNCD. A gas system, with hydrogen completely replacing Ar as the majority gas composition, and a methane/hydrogen ratio significantly higher than that in the conventional chemical vapor deposition polycrystalline diamond recipe, is introduced to enhance renucleation rate, which is different not only from conventional UNCD deposition which employs Ar, but also from conventional polycrystalline diamond deposition which utilizes a carbon/hydrogen ratio as low as 0.1-0.3 %. [7]. Especially, in this H-rich gas system without Ar, high levels of boron doping has been realized in UNCD, which is the focus here.

As an emerging P-type material, boron-doped diamond (BDD) combines the desirable mechanical properties of diamond with the additional advantages of a wide band gap [8], and a wide potential window with very low background currents when used as electrochemical electrode [9]. With a similar bonding structure to natural diamond, BDD shows extremely high chemical, biochemical, and electrochemical stability. These properties enable BDD to achieve wide application in the advanced oxidation of harmful chemicals or pathogens [10], On-Site Generation (OSG) for chlorine and mixed-oxidants, [11-13] and high sensitivity

biosensing [14-16] especially in harsh environments or *in vivo* testing conditions where extreme chemical and physiological inertness is desirable. However, most of the BDD discussed in the literature is the much rougher (and less physiologically inert) NCD or MCD, [17] with surface roughness values in excess of 100 nanometers. The rough as-deposited surfaces of these materials complicates further processing or patterning by high resolution photolithography, as well as bonding, or its integration into more complex structures. Although diamond surfaces inherently possess attractive tribological properties [18-20] and high biocompatibility [21-22], the roughness of NCD and MCD actually diminish their overall tribological and biological compatibility.

While nitrogen-doped UNCD has been studied previously, [23-24] boron-doped UNCD (BD-UNCD) has not been systematically described and characterized in the literature. Swain's group reported the smoothest boron-doped diamond yet reported by adding a boron source (solid state BoronPlus and gas state B_2H_6) to conventional Ar-rich UNCD gas system. They achieved BDD with a minimum roughness of 34 nm and a resistivity on the order of 0.1 ohm·cm. [25] The present authors began developing boron-doped UNCD in 2009, targeting a super smooth, heavily doped UNCD film as a standard material to enable micro- and nanotechnology for MEMS and other devices, electrochemistry and biosensing applications. Through the use of an Ar-free gas strategy, heavily boron-doped UNCD with a resistivity as low as 0.01 ohm·cm was developed, with almost as low a surface roughness as un-doped UNCD. Since then, such BD-UNCD has been used to fabricate piezo-resistive microcantilevers [26], conductive atomic force microscopy probes, electrochemically stable electrodes and biosensors. To date, there is no report in the literature describing in detail the properties of BD-UNCD. Here, we discuss the film synthesis of BD-UNCD and address differences between BD-UNCD and conventional BDD, with emphasis on its signature properties revealed by scanning electron microscopy (SEM), transmission electron microscopy (TEM), Raman spectroscopy, and Near Edge X-ray Absorption Fine Structure (NEXAFS), and Atomic Force Microscopy (AFM) etc. Typical applications of this versatile diamond film are also discussed.

2. Experimental Section

2.1 BD-UNCD Synthesis. BD-UNCD is deposited at Advanced Diamond Technologies, Inc. A hot-filament chemical vapor deposition (HFCVD) reactor is used for the deposition.

Diamond film synthesis begins with substrate seeding with commonly used seeding processes such as surface mechanical abrasion with diamond particles or sonication with slurries containing suspended diamond nanoparticles, [27]. A high density of diamond particles (usually 10^9-10^{12}/cm^2) on the substrate ensures appropriate seeding density which accelerates the onset of deposition and provides for a more uniform growth rate and thickness across the substrate. The reactor setup and seeding processes are similar to those reported in the prior art [28-29]. The major difference here is that we employ a H-rich gas system with a CH_4/H_2 ratio as high as 10%, which is much higher than that of the previously reported polycrystalline diamond with high sp3 purity and the chamber pressure is set lower than in the literature, i.e. < 15 Torr. The substrate temperature is in the range of 400˚C-850˚C, as monitored by thermocouples with their tips touching the back side of the witness Si chips. Deposition rates are in the range of 0.5-3 μm/hour, depending on coating temperature and loading area. The boron doping source is gaseous trimethylborane (TMB, i.e., $B(CH_3)_3$) premixed with very high ratio of hydrogen (> 95%). Boron-to-carbon ratio in the gas mixture (brief as B/C gas ratio in this paper) can be in a wide range from 0-13000 ppm. Without specific notes, the samples in this work were prepared with 5 Torr chamber pressure, 750 °C substrate temperature and 3000 ppm B/C gas ratio.

2.2 Characterization. The resistivity of the BD-UNCD as deposited was measured on 1-μm thick thermal oxidized Si wafers up to 12 inch in diameter (see insert of Fig. 1), with a Four Point Resistivity System (Lucas Labs Pro-4). High resolution SEM and TEM were used to study grain and surface morphology of the BD-UNCD. The accelerating voltage, aperture size and working distance of the SEM were 10 kV, 10 μm and 10 mm, respectively. Transmission electron microscopy (TEM) was performed on atomic force microscope tips composed of BD-UNCD. Multiple probes with nominally identical geometries were fabricated from both materials using the molding technique described in [30], which results in sharp monolithic UNCD tips. The probes were imaged using a JEOL 2010F TEM with a field-emission source, using an accelerating voltage of 200 kV. The back sides of the cantilevers were sputter-coated with 100 nm of aluminum to enhance conductivity and prevent charging in the TEM. In addition, a small amount of conductive epoxy was applied to ensure electrical connection between the UNCD and the TEM sample mount. The Raman spectra were obtained using a spectrometer (Control Development 2DMPP) with an excitation laser wavelength of 532 nm. The NEXAFS measurements were performed at the National Synchrotron Light Source (NSLS) at Brookhaven National Laboratory (BNL,

Upton, NY). Two beam lines, U7A and U12A, were both employed for acquiring spectra on as-grown UNCD and BD-UNCD films. The photon source of these beam lines is a bending magnet, and which permits a wide spectral energy range from 100 to 800 eV. The photon flux was $2x10^{11}$ photons/second/0.1% bandwidth, with a resolution of ~$1x10^{-3}$. All measurements were carried out in partial electron yield (PEY) mode at a photon incidence angle (relative to the sample surface) of 90º. The spectra acquired with the U7A beam line were first normalized to the absorption current measured simultaneously from a gold mesh placed in the beam line upstream from the analysis chamber, and then normalized based on the absorption in the post-edge region (at 320 eV). The spectra acquired at U12A were first normalized to the absorption current measured under the same experimental conditions as those from U7a on a sputter-clean platinum sample, and then normalized based upon the absorption in the post-edge region (at 320 eV). The quantification of the sp^2 fraction from NEXAFS spectra was performed following the approach described in [31]. Atomic Force Microscopy (AFM, Veeco Nanoscope IIIa) was employed to study the roughness of BD-UNCD. An AFM tapping mode was used to scan a 5 μm×5 μm area to extract the root mean square (RMS) roughness.

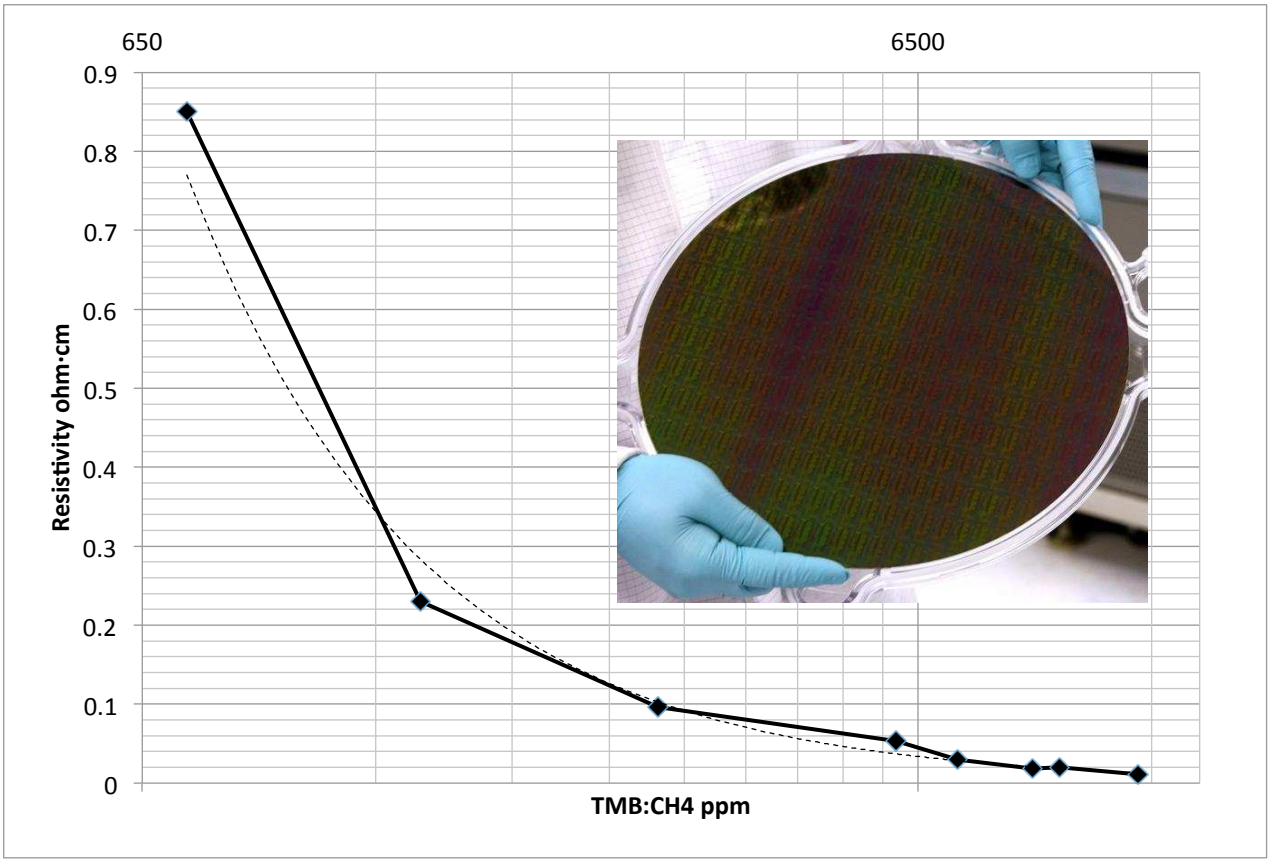

Fig. 1 Resistivity vs. B/C gas ratio in gas mixture. Dash line represents a reciprocal curve with a reciprocal constant of 300 ohm·cm·ppm. Error of all data is < 10% except at 750 ppm which has an error of 20%. The insert shows a 12-inch BD-NUCD wafer under test.

3. Results and discussions

3.1 Electrical properties. Fig. 1 depicts the relationship between resistivity and B/C gas ratio. This relationship approaches a reciprocal trend, with a reciprocal constant at ~ 300 ohm·cm·ppm. When the B/C gas ratio increases to range of ~ 9000 to 12500 ppm, the resistivity tends to saturate at 0.01 ohm·cm. When the B/C gas ratio reaches 15000 ppm or higher, the resistivity increases significantly to about one order of magnitude, to 8×10^{-3}-3×10^{-4} ohm·cm, corresponding to a film structural change from diamond to graphite, which is confirmed by other characterizations below. At the lower doping end of the graph, when the B/C gas ratio decreases to 1000 ppm and less, the resistivity increases to > 0.8 ohm·cm. Resistivity determinations becomes more difficult when the B/C gas ratio decreases further, since the background boron contamination remaining in the reactor from other depositions introduces unaccountable errors in the estimation of the actual boron content in the gas mixture. As a reference, the resistivity of undoped UNCD, produced by a reactor never used for boron doping, was measured higher at 10^6 ohm·cm.

Since the authors did not have access to secondary ion mass spectrometry (SIMS) a comparative measurement on the conductivity (the inverse of resistivity) vs. B/C gas ratio was conducted between the data presented here and the data from the literature for boron doped NCD [32]. At a B/C gas ratio of 6660 ppm, the reported conductivity for the heaviest doping is 76 s/cm, while by contrast, the BD-UNCD conductivity measured here was 100 s/cm for the heaviest doping level at 12500 ppm, which is comparable with the literature value. This conductivity corresponds to a dopant concentration on the order of $10^{21}/cm^3$. Such a heavy doping level likely arises from the presence of heavy boron concentrations at the incredibly large internal surface area of UNCD grain boundaries [33]. The carbon atoms on the boundary interfaces and in the boundaries themselves are expected to exhibit more dangling bonds to retain the boron dopant atoms than inside the grains themselves. A detailed study of the doping at the boundary based on actual SIMS data is required to substantiate this hypothesis.

3.2 Grain and morphology. Figure 2a-g depicts BD-UNCD morphologies under high resolution SEM as obtained from different B/C gas ratios. The top view SEM images of heavily doped BD-UNCD (Fig. 2b-f) usually show line-granular structures on the surfaces of the films, rather

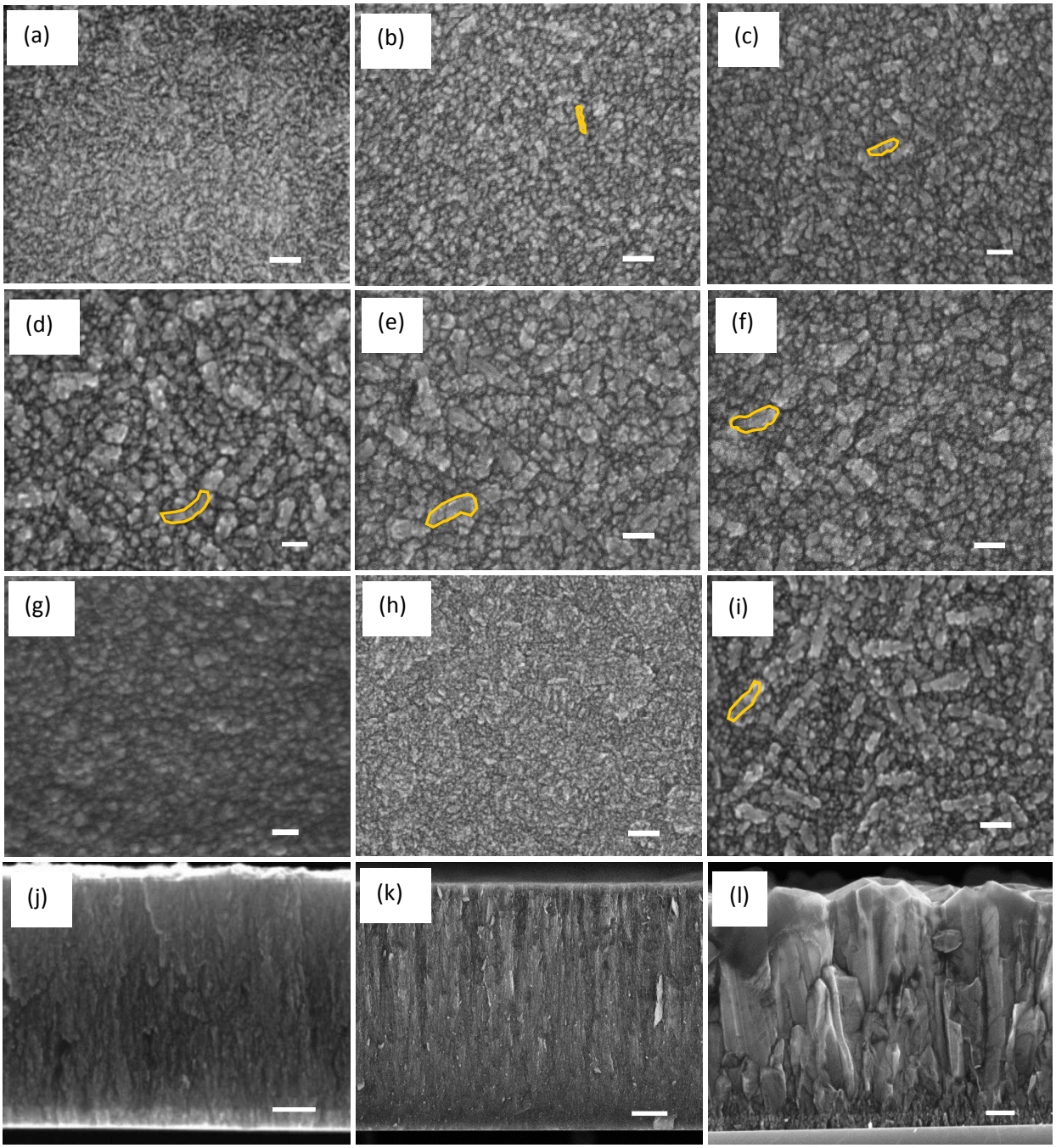

Fig. 2 SEM images of UNCD with B/C gas ratio of (a) 0 ppm i.e. undoped, (b) 750 ppm, (c) 1500 ppm, (d) 3000 ppm, (e) 6000 ppm, (f) 9000, (g) 12500 ppm, and of (h) Nitrogen doped UNCD. Film thickness in of samples in (a)-(h) is 1 µm; (i) UNCD with 3000 ppm B/C ratio, but with 10 µm thickness, and cross section images of (i) UNCD with 3000 ppm B/C ratio and 1 µm thickness, (j) UNCD with 3000 ppm B/C ratio and 10 µm thickness, and (i) MCD with 3000 ppm B/C ratio and with 1.5 µm thickness. Orange marks outline the line-granular structures of BD-UNCD. Scale bar in (a)-(i) represents 100 nm, (j) and (l) represents 200 nm and in (k) represents 2 µm.

than the faceted grains of conventional NCDs, which is also different from un-doped UNCD

(Fig.2a) and nitrogen doped UNCD (Fig.2h). These line-granular structures contain many grains. The size of the line-granular structures increases as the B/C gas ratio increases until the B/C ratio reaches 9000 ppm. It is hypothesized that such an increase may arise from a slightly increased grain size, similar to that reported from the deposition of nitrogen doped UNCD, when the nitrogen concentration is increased. [24] However, no obvious facets of crystallites could be seen under SEM even with a magnification of 100,000 ×. At boron concentrations above 9000 ppm, the size increase of the line-granular structure does not increase significantly with increasing boron concentration. When the B/C gas ratio increases to 13000 ppm, the film texture starts to change (Fig. 2d), which suggests the onset of graphitization. The typical BD-UNCD line-granular texture shown in Fig 2b-f is preserved as long as the deposition is conducted at deposition temperatures between 600-800 ˚C. The detailed mechanism for the formation of such a special structures is not yet known. When the deposition is conducted at a temperature lower than 600 ˚C, the facets of crystallites become much more evident under SEM as reported in ref [34].

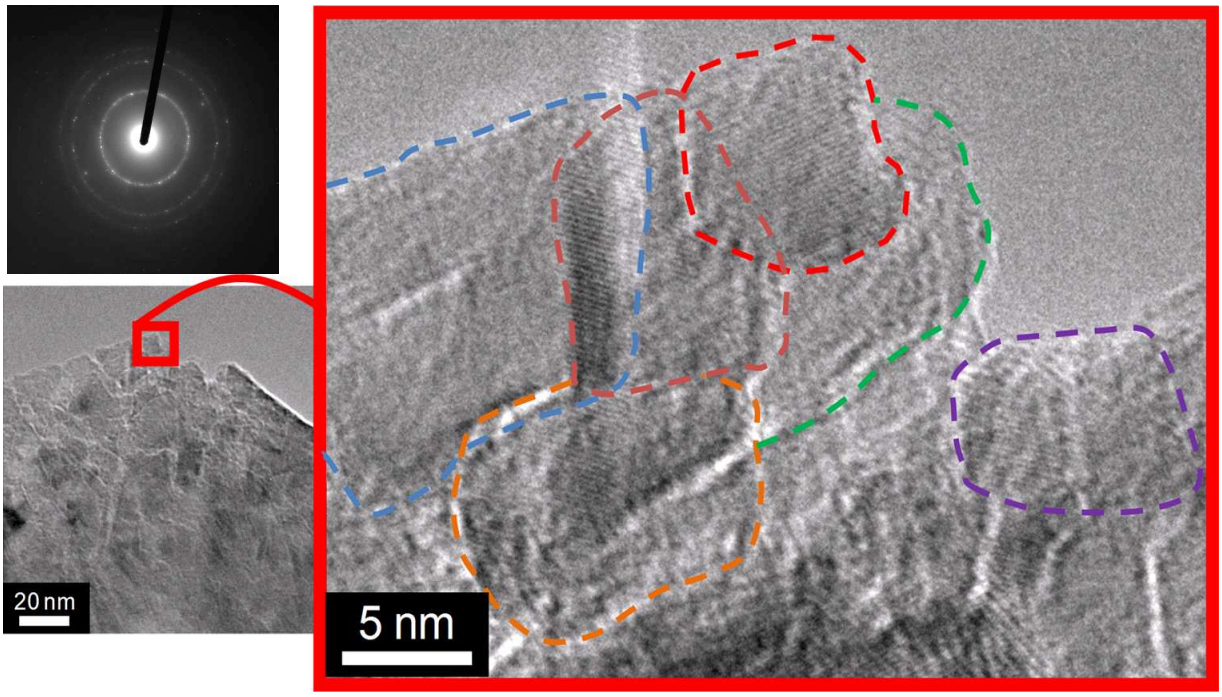

Fig.3 Representative TEM images showing AFM probes composed of BD-UNCD. Individual grains are readily discerned from lattice fringes and contrast variations. For clarity, colored dashed lines have been superimposed on the image to identify grain boundaries. Because this is a three-dimensional structure, grains can appear to overlap one another. The B/C ratio of the BD-UNCD in the figure is 3000 ppm. The electron diffraction pattern of BD-UNCD is shown at the upper left corner.

It is interesting that this line-granular structures size and shape do not significantly change when the thickness is increased from 1 μm (Fig. 2d) to 10 μm (Fig. 2i). The cross sectional SEM images of the BD-UNCD films confirms that the topography of BD-UNCD remains smooth over a thickness range from submicron to 10 microns (Fig. 2j-k), which is a feature specific only to UNCD. This is, in contrast to MCD whose topography dramatically increases as the film grows (Fig. 2l). It should be noted that BD-UNCD is optically darker than undoped UNCD and NCD, and therefore its thickness is difficult to determine by means of reflectometry due to low signal if the film thickness is more than 1 μm. The thickness is usually measured by cross-sections of witness chips and visualizing the layer under either optical or electron microscopy. The detailed mechanisms for such high absorption is unknown, but one explanation is that the concentration of boron at the abrupt grain boundaries increases light absorption. Thickness measurements demonstrate that the deposition rate of BD-UNCD is 5-30% higher than that of un-doped UNCD. Bright-field TEM images, as shown in Fig. 3, enable visualization of individual crystalline grains within the BD-UNCD. TEMs on AFM probes fabricated from BD-UNCD, with a B/C ratio of 3000 ppm, show grain diameters ranging from 5-15 nm, in accordance with previously published undoped UNCD [2] or slightly larger. The insert diffraction pattern in Fig.3 consists of continuous and smeared-out circles with smaller bright dots, suggesting randomly oriented small grains of UNCD similar to those reported produced using Ar-rich gas mixtures. [2]

3.3 Raman spectrum Fig. 4 shows a comparison of Raman spectra for B/C gas ratios of: 0 (undoped), 750, 1500, 3000, 6000, 9000, and 12500 ppm. The Raman signal intensity decreases as the B/C gas ratio increases. Therefore, the signals for films obtained with 0-3000 ppm and films with 6000-12500 ppm B/C gas ratio are represented in separate graphs (Fig. 4a and 4b, respectively) such that the spectrum details for each ratio are evident. In Fig. 4a, there are four peaks at 1150, 1310-1355, 1470, 1560 cm^{-1}, similar to those reported by Swain's Group. [25] However, there are two major differences from that work. The first difference is that there is no sharp peak around 1333 cm^{-1}, suggesting a shortage of large size grains and enriched grain boundaries of UNCD. [35] Actually, in this range there is a wide "hybrid" peak combining a weak peak of first order of sp3 (1333 cm^{-1}) and a more dominant so-called "D band" peak (1310-1450 cm^{-1}). [36] As the B/C gas ratio increases, the center of the peak shifts from 1355 cm^{-1} (B/C = 0 ppm) to ~1300 cm^{-1} (B/C = 6000 ppm), similar to ref. [32]. Although the peak shift of the first order of sp3 has been explained well, the shift of the D band peak along with boron concentration has not yet been explained. Such a shift may

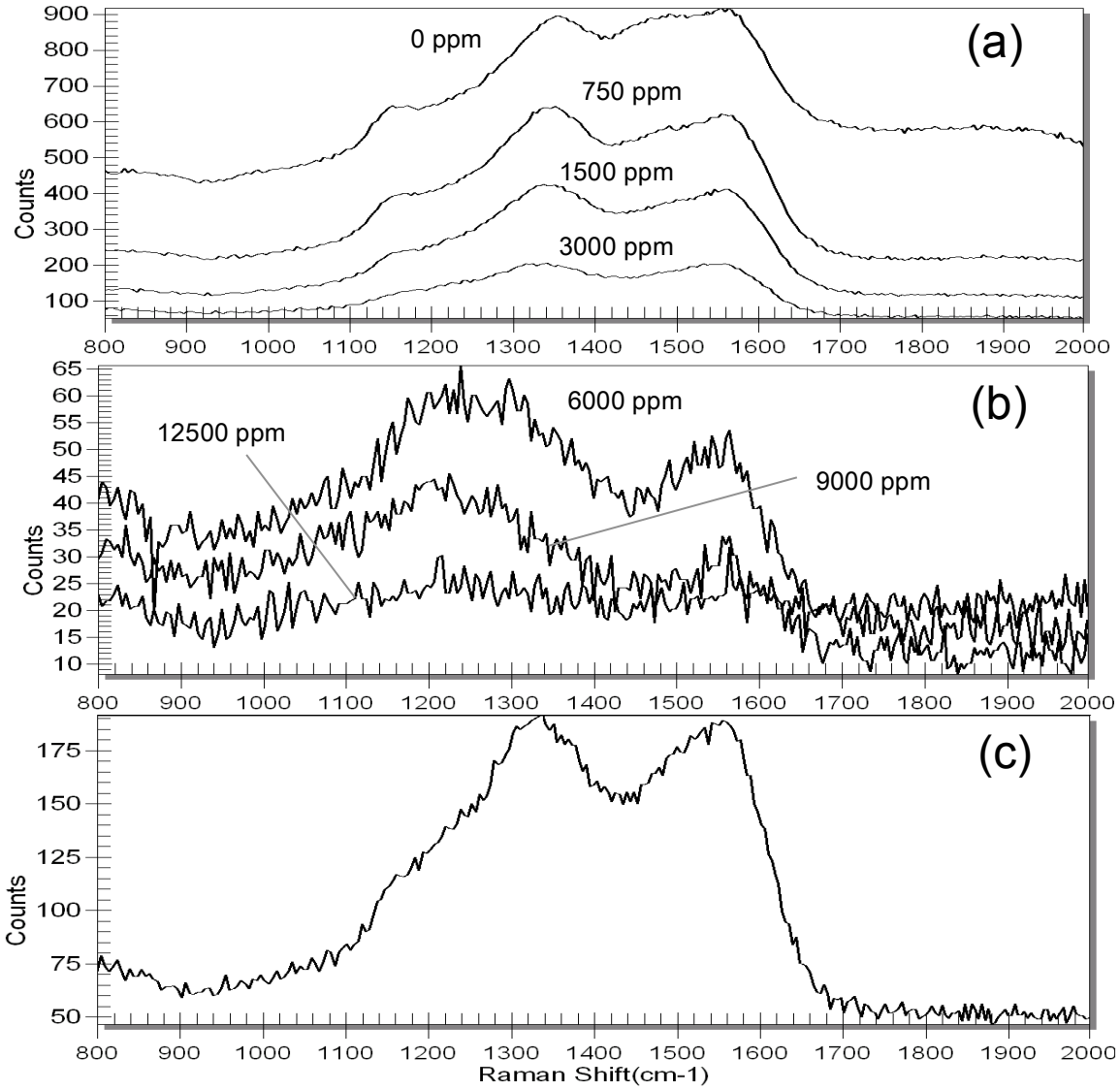

Fig.4 Raman spectra of BD-UNCD with B/C gas ratio of (a) 0-3000 ppm, (b) 6000-12500 ppm and (c) 3000 ppm-only for best contrast.

be caused by content changes at the grain boundary where B-C bonds are dramatically increased. It is known that in UNCD, most of the disordered carbon, represented by the D peak in a Raman spectrum, is confined to the grain boundary, therefore the introduction of excessive boron concentrations at the grain boundary could change the distribution and properties of the disordered carbon.

The second difference in the Raman spectrum from the prior art, are the peaks at 1150 cm^{-1} [37-38] and 1470 cm^{-1} (1450 cm^{-1} as in [38]) according to the work of Show et al. [25] These peaks are evident only in undoped UNCD and low B/C gas ratio H-rich/Ar-free BD-UNCD in this paper, but become weaker when the B/C gas ratio increases. This was also observed in

boron doped NCD and MCD, [32] and was explained as a decrease of hydrocarbon content or hydrogen termination. Ferrari's assignment of the 1150 cm^{-1} and 1470 cm^{-1} to ν_1 and ν_3 modes of trans-polyacetylene, suggests that the amount of transpolyacetylene decreases as the boron doping level increases. When the B/C gas ratio reaches 3000 ppm, the Raman spectrum of BD-UNCD is dominated by only two major peaks, i.e., the D peak at 1310-1350 cm^{-1} and the G peak at 1560 cm^{-1},featured as an "M" shaped Raman spectrum as shown in Fig. 4c, with a B/C gas ratio 3000 ppm shown as an example. The "M" shape Raman spectrum was somewhat surprising, since a D- and G-peak dominated Raman spectra was usually attributed to a combination of a high percentage of graphite and disordered carbon, but actually, evidence collected from SEM, TEM above and NEXAFS data below, ruled out this suspicion.

As the B/C gas ratio reaches 6000 ppm, it is noted that one of the two peaks of the "M" shape spectrum shifts from 1310-1350 cm^{-1} to 1220 cm^{-1}, as shown in Fig. 4b, while the peak at 1560 cm^{-1} is unaffected. Many authors reported a peak at 1220 cm^{-1} for heavily doped nano- or microcrystalline diamond Raman spectra, but the explanations for this peak are diverse. [32, 39-41] As mentioned above, in this study no obvious facets of crystallites were seen under SEM even with a magnification of 100,000 ×. It is easy to distinguish the Raman signature of BD-UNCD from that of boron doped MCD, since the Raman spectrum of BD-UNCD has an "M" shape signature, while the Raman spectrum of heavily doped MCD only has one major sharp peak at 1220 cm^{-1}, without a G peak from the grain boundaries, like "Λ" shape. In ref. [34], the authors observed that boron does assist in the generation of larger grains, but the presence of boron must be combined with very low deposition temperatures (< 500 ˚C). When the B/C gas ratio is 15000 ppm or greater, the Raman spectrum acquires a signature typical of being evidently graphitized, which is compatible with SEM observations.

3.4 Near-edge X-ray absorption fine structure (NEXAFS) spectroscopy. NEXAFS is sensitive to oxidation state, hydrogenation, hybridization, and local ordering. It was used to gain insight into the bonding configuration of carbon in BD-UNCD and to compare it with that of undoped UNCD. The carbon 1s NEXAFS spectrum of undoped UNCD, shown in Fig. 5a, exhibits the characteristic features of diamond [42], namely the edge jump at ~289.0 eV, the exciton peak at ~289.3 eV, and the second band gap at ~302.5 eV. All these features are due to the C 1s $\rightarrow \sigma^*$ transition for sp^3-hybridized carbon-carbon bonds in the crystalline

diamond configuration. Besides the characteristic peaks of diamond, a small absorption band at 285.0 eV was detected. This can be assigned to the C 1s $\rightarrow \pi^*$ transition for disordered sp^2-hybridized carbon-carbon bonds. The sources of this sp^2-bonded carbon are surface contamination, surface reconstruction, and grain boundaries within the UNCD [42]. The

presence of a subtle shoulder at ~287.5 eV can be attributed to the C 1s → σ* transition for C-H bonds, indicating hydrogen termination of the UNCD surface. [19, 43]

The characteristic NEXAFS spectrum of BD-UNCD (grown at the same temperature, *i.e.,*

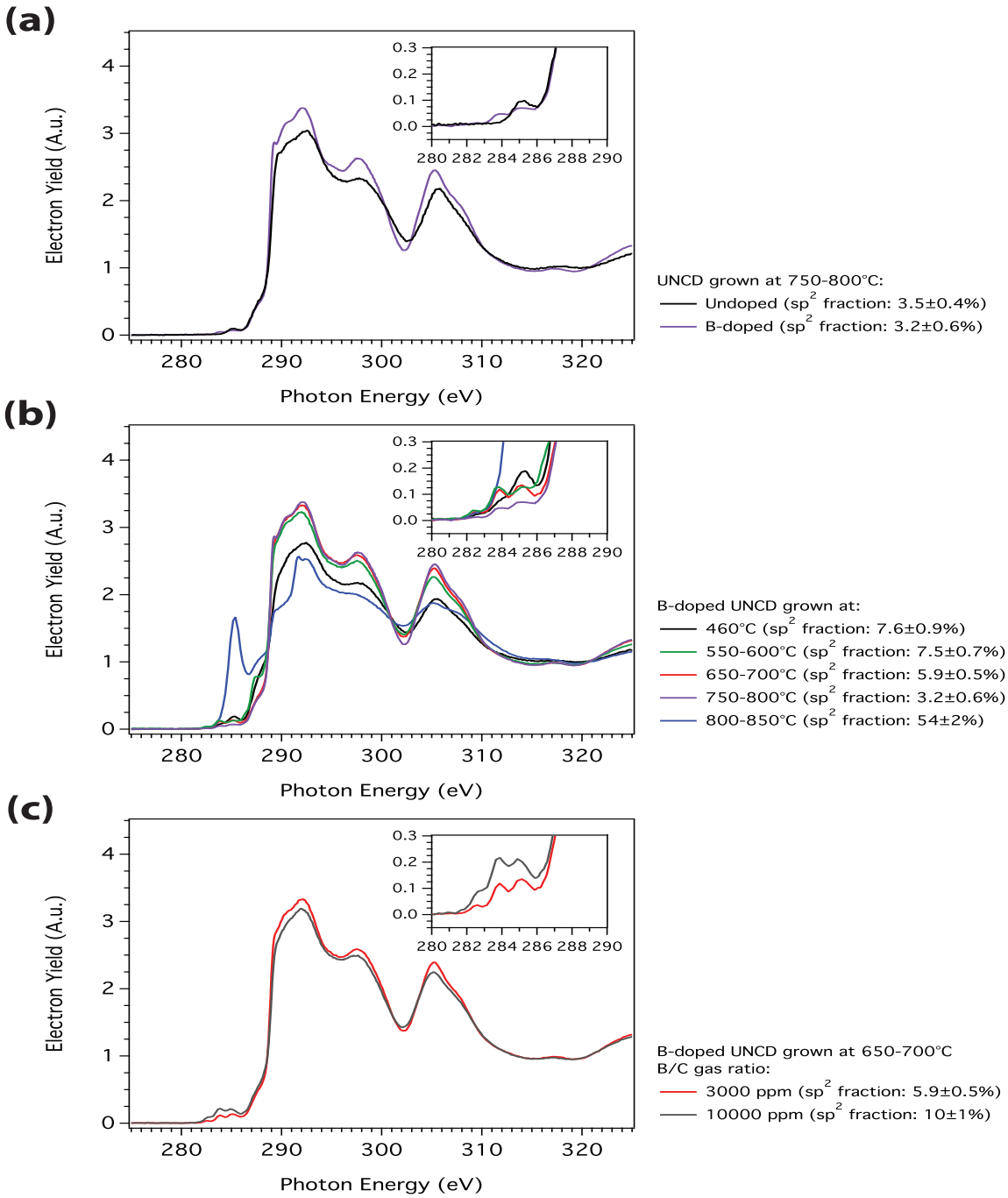

Fig 5. C 1s NEXAFS spectra of: (a) undoped and BD-UNCD grown at the same temperature (*i.e.*, 750-800°C); (b) BD-UNCD films grown at different temperatures. B/C gas ratio = 3000 ppm; (c) BD-UNCD films grown at 650-700ºC with different B/C gas ratios. The fraction of sp^2-hybridized carbon is reported in the legend.

750-800°C as the undoped UNCD, in Fig. 5a exhibits all the characteristic diamond features listed above. Doping UNCD with boron did not affect the fraction of sp^2-bonded carbon in the film, but resulted in a subtle change in the absorption of the C 1s $\rightarrow \pi^*$ transition for disordered sp^2-hybridized C-C bonds. In contrast, for undoped UNCD this feature is symmetric, and upon boron-doping a second band appeared at lower photon energies (~283.8 eV). The detection of this second peak might be attributed to the presence of unoccupied gap states lying below the π^* band.

The effect of deposition temperature on the local bonding configuration was also investigated by NEXAFS spectroscopy. The NEXAFS spectra of BD-UNCD, with a constant B/C ratio of 3000 ppm, grown at temperatures ranging from 460°C to 850°C exhibit significant changes (Fig. 5b). In particular, the fraction of sp^2-bonded carbon was found to slowly decrease, down to 3.2%, upon increasing the deposition temperature up to 800°C. For deposition temperatures above 800°C, the fraction of sp^2-hybridized carbon in BD-UNCD films significantly increases. The deposition temperature also affected the amount of hydrogen in the near-surface region: upon growing the films at lower temperatures (460-600°C), the intensity of the shoulder at ~287.5 eV, attributed to the C 1s $\rightarrow \sigma^*$ transition for C-H bonds, increases. This indicates that the number of C-H bonds formed at the UNCD surface is higher at lower deposition temperature than that of films deposited at higher temperatures. However, when the temperature is in the range of 650°C to 800°C, the C-H bond density becomes constant. Changing the growth temperature also resulted in a variation in the absorption of the C 1s $\rightarrow \pi^*$ transition for disordered sp^2-hybridized C-C bonds. In addition to the band at ~283.8 eV, which was detected in all the spectra of BD-UNCD films independently of the deposition temperature, the NEXAFS spectra of BD-UNCD films grown at temperatures below 750ºC exhibited an additional feature at ~282.3 eV attributable to this C 1s transition.

Fig. 5c shows the impact of different B/C gas ratio on the diamond chemistry. It suggests that the fraction of sp^2-bonded carbon in the UNCD film is influenced by the B/C gas ratios: upon increasing this ratio, e.g. from 3,000 ppm versus 10,000 ppm, which corresponds to increasing the amount of dopant in the film by roughly three-fold, the fraction of sp^2-bonded carbon only slightly increases. However, the intensity of the shoulder at ~287.5 eV, attributed to the C 1s $\rightarrow \sigma^*$ transition for C-H bonds is not changed by B/C ratio. Since Fig. 5b

demonstrates that the 287.5 eV shoulder does not change with the diamond deposition temperature between 650 °C and 800 °C, combining Fig. 5a and 5c, one can conclude that the 287.5 eV shoulder is actually unchanged in the whole range of B/C gas ratios, from 0 ppm (undoped) to 10000 ppm. The BD-UNCD features 3 peaks at 282.3 eV, 283.8 eV, 285.0 eV, the C 1s $\rightarrow \pi^*$ transition for disordered sp^2-hybridized carbon-carbon bonds appear in both levels of B/C gas ratios, except the height of these peaks increases with almost the same ratio as the B/C ratio increases.

3.5 Surface roughness.

The dependence of surface roughness versus film thickness was also studied. This study shows a merely linear dependence, from a very low value of 8 nm RMS at 0.5 μm thickness to 44.5 nm RMS at 13 μm thickness, comparable or slightly smoother than previous work. [25] This demonstrates that the roughness of BD-UNCD increased very slowly as the thickness increases, comparable to that of standard undoped UNCD, suggesting its roughness is much less dependent on thickness than NCD or MCD. As a comparison between BD-UNCD and BD-NCD, Fig. 6a and 6b show AFM images of a 1-μm-thick BD-UNCD and BD-NCD with 8 nm and 76 nm RMS roughness respectively. For UNCD, the surface roughness of a diamond film is determined by the renucleation rate and the crystalline growth rate. If the renucleation rate is much higher than the crystalline growth rate, theoretically the diamond would be very smooth. Therefore, if required, by further adjusting the gas (CH_4, H_2, and TMB) ratios and the reactor pressure to target a faster the renucleation rate, an even smoother BD-UNCD of thick films can be expected. Starting from an already low as-deposited surface roughness, BD-UNCD can be polished to sub-nanometer roughness much more easily and cheaply than BD-NCD or MCD. An AFM image of a polished BD-UNCD surface with RMS roughness of less than 1 nm is shown in Fig. 6c. Roughness variations with controlled B/C gas ratios have also been studied. The roughness of films with a standard 1 μm thickness and different B/C gas ratios ranging from 0 ppm to 12500 ppm was measured and is presented in table I. It is interesting that no significant correlation between surface roughness and B/C gas ratio can be observed, while all these films display roughness values typical of UNCD. Even the SEM images (Figure 2a-f) demonstrate the size of the line-granular structure and so possibly the grain size increases when the B/C gas ratio increases. This suggests that the grain size difference caused by the boron is too small to contribute significantly to the surface roughness.

B/C gas ratio (ppm)	0	750	1500	3000	6000	9000	12500
RMS (nm)	6.8	6.6	6.5	7.4	6.8	7.5	6.9

Table 1: Surface roughness vs. B/C gas ratio. Each roughness value is an average from 5 points across a 4 inch BD-UNCD coated wafer.

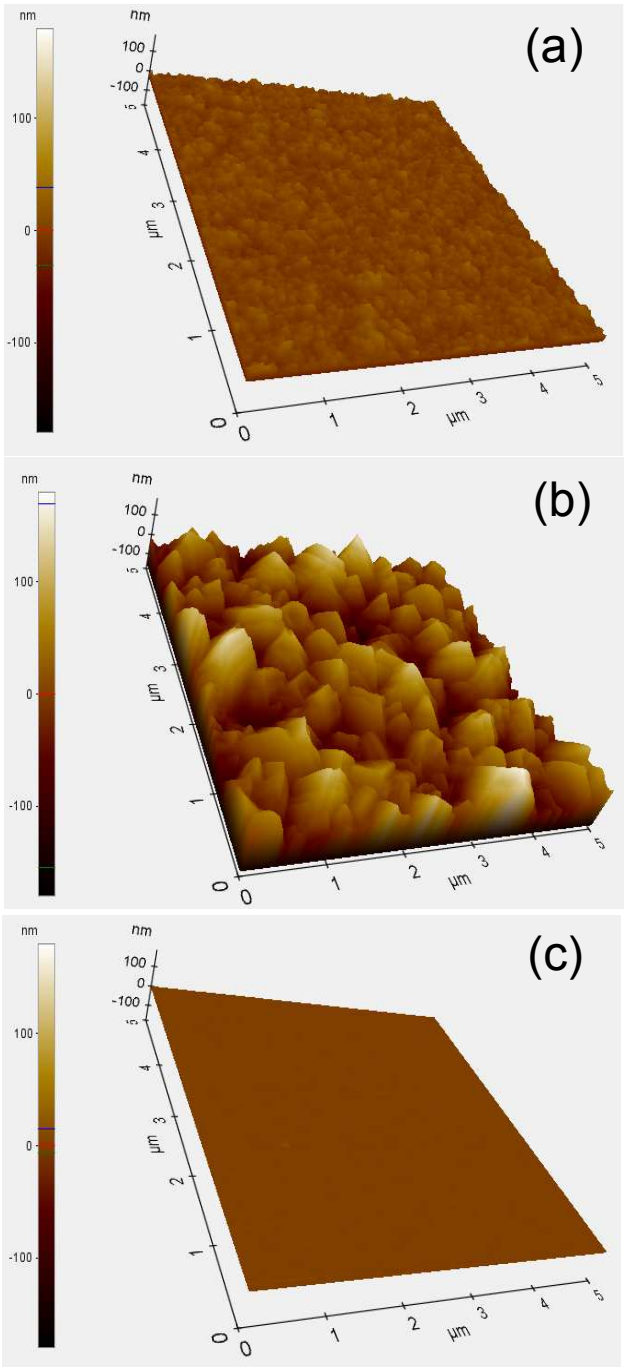

Fig. 6 AFM images of (a) BD-UNCD, (b) BD-NCD and (c) CMP smoothened BD-UNCD. All images are capture via Tapping Mode within 5µm×5µm^2.

3.6 Role of hydrogen

From the data presented above, it can be deduced that the boron doped diamond films described in this report belongs to the UNCD type. They feature very low surface roughness,

low correlation between surface roughness and thickness, as well as a non-facet texture under SEM, and very small grain size as determined by TEM. In addition, according to the NEXAFS results, it can be concluded that the sp3 purity of the BD-UNCD is roughly equivalent to that of undoped UNCD reported previously in the literature. More importantly, undoped and doped UNCD can be fabricated with H-rich gas chemistry instead of an Ar-rich gas chemistry. In a PECVD system, Ar makes the plasma very hot, which generates more precursor species. However, in the HFCVD system, the precursor species are generated by the high temperature of the filament, so the involvement of Ar is unnecessary. The role of Ar in a PECVD reactor for UNCD synthesis is replaced by hot H atoms cracked from H_2 gas. The energy for the cracking in the HFCVD reactor is provided by the heat obtained from the hot filament (at temperatures up to ~2400 °C). The major functions of the hot hydrogen are: 1) Reacting with and removing sp2 carbon from the growing diamond film, 2) in a gas system when boron is present, facilitating access to the diamond surface for the boron to react with carbon more efficiently than Ar due to its smaller size and 3). Transferring energy to radicals and precursor species (such as CH3.), which enhances and accelerates the formation of the UNCD film.

It should be noted that that the high sp3 percentage (diamond purity) of BD-UNCD can be realized in a high methane H-rich gas chemistry. This is in contrast to the previous-reported chemistry used for UNCD, NCD and MCD, i.e., the present work shows that high CH_4/H_2 ratio is not necessarily connected with low sp3 purity. Conventional NCD or MCD depositions typically use CH_4/H_2 gas mixtures, while very low CH_4/H_2 ratios are required. To ensure high sp3 purity, the flow rate of CH_4 in NCD/MCD deposition is recommended to be less than 0.5%, otherwise “dirty diamond” would be produced. [7, 25] For example, even 1-3% CH_4/H_2 ratio would result in up to 50% sp2 impurities. [27]. However, the present study demonstrates that UNCD, especially BD-UNCD can be achieved not only in H-rich/Ar-free gas system, but also in a gas system with a high concentration of methane (up to 10%), which underscores the fact that a CH_4/H_2 ratio is not crucial for diamond quality. The work presented here is guided by a simple hypothesis: that as UNCD is a form of diamond with a much higher deposition renucleation rate than NCD or MCD, therefore any methods to maintain a sufficiently high renucleation rate, such as Ar addition, higher CH_4/H_2 ratios or even instant pressure changes, may all allow the deposition of a UNCD film. However, simultaneously with high renucleation, deposition of non-diamond carbon phase also exists. The key aspect differentiating between these methods is the method of removal of the non-

diamond carbon and other hydrocarbon "scum" produced during renucleation. In the Ar-rich system, c-dimers may directly lead to diamond lattice construction, with minimum "scum" generation. For the H-rich system, although "scum" is generated during the renucleation, if the filament temperature is high enough, abundant hot H-atoms can be generated to remove the "scum", i.e. react with the non-diamond carbon and hydrocarbons, which leads to gaseous products that are able to be pumped away. As NCD was considered as a thinner version of MCD, [44], previous work using similar deposition conditions to that of MCD have been used to produce NCD, which may lead to high levels of sp2 impurities. For example, reactor pressures were usually set high, typically > 30 Torr. [45-46] which is more suitable for MCD fabrication but may be a factor causing formation of excessive non-diamond carbon during deposition of the film. Therefore high sp2 content has usually been reported when the concentration of the carbon-based gas was high. In the work presented here, the BD-UNCD deposition process employs a high CH_4/H_2 ratio and reactor pressure below 15 Torr, which ensures both a high diamond renucleation rate and a high non-diamond carbon removal rate. While maintaining such a low pressure and decreasing the CH_4/H_2 ratio to 0.5-2%, it was found that the diamond naturally transitions to a nanocrystalline form, but with <5% sp2 content measured by NEXAFS (not shown here), much lower than has been reported with the similar CH_4/H_2 ratio. [25, 47] With the hypothesis of "scum removal", the authors are able to explain that under lower pressure, hydrogen removes more non-diamond components (hydrocarbons and sp2 carbon etc.) to ensure a higher purity of sp3 deposition.

This report provides an alternative method to fabricate UNCD with an H-rich/Ar-free gas system. This does not suggest that the H-rich method will entirely replace the conventional Ar-rich method, since the molecular dynamics in the deposition require further study. However, the HFCVD UNCD method provides substantial advantages in the area of large area deposition and reduced capital cost for the reactor. In addition, the H-rich and HFCVD approach allows a much better overall understanding of the deposition mechanisms for UNCD under these deposition conditions and for those of the Ar-rich PECVD system.

It is also speculated that, by avoiding the use of Ar and its high ionization rate, the rate of boron-carbon interaction may increase, especially at the grain boundaries, thus readily realizing a heavy boron doping in UNCD in the HFCVD system is easier than in PECVD systems. Since the mass of an Ar atom is larger than that of B, in an Ar-rich gas system, the B-C reaction is significantly hindered by Ar atoms. The kinetic energy of B atoms in the Ar-

rich system can be easily changed by collisions with Ar atoms; however, in the H-rich system, since the mass and volume of an H atom is much smaller than a B atom, H atoms affect the behavior of B to a lesser degree. For doped UNCD, a popular model is that the grain boundary accommodates the majority of the dopant. [33] In the narrow confines of diamond grain boundaries, H atoms in the Ar-free HFCVD system, interfere less with boron attachment to carbon's dangling bonds than the larger and more energetic Ar atoms in the Ar-rich PECVD system. Therefore, it is hypothesized that it is easier for an H-rich gas system to realize heavy boron doping and high conductivity UNCD than the Ar-rich PECVD system. This is more significant when low temperature depositions are required, e.g. for semiconductor applications with metallization already present on the wafer, in which the concentration of the precursor species near the substrate to be coated is very low and the presence of Ar may be even more "disturbing" both to diamond growth and B-C bond formation. In addition, when H atoms collide with B atoms, they tend to elastically recoil with the same or similar kinetic energy. Thus, boron bond formation is not disrupted. In contrast to Ar, even though its kinetic energy is low, the chemical reactivity of H atoms is very high for sp2 carbon and hydrocarbons which would otherwise form on the surface of the growing diamond film. Thus the relative efficiency for "scum removal" is very high for H atoms as compared to Ar, while the interference with boron bond formation with diamond's dangling bonds is low due to the low kinetic energy of H as compared to Ar. Since Ar does not tend to form bonds with carbon, its ability to chemically remove "scum" from the surface of the diamond is minimal. The above hypothesis for the mechanism by which H can facilitate BD UNCD formation is inferred from the known properties of these two atoms. However, further detailed research to quantify these mechanisms would be interesting and useful.

4.Applications

The BD-UNCD films described above are already being used commercially, with deposition on wafers up to 12 inches in diameter as shown in the insert of Fig.1. High thickness uniformity (> 90%, and as high as > 98% across 12" substrates), low roughness and controllable intrinsic stress (both tensile and compressive) enable the application of diamond in MEMS or even NEMS fabrication, with very tight manufacturing tolerances. A series of applications of BD-UNCD have been developed since 2009, including pure monolithic and coated BD-UNCD probes for scanning probe microscopy, electrodes for direct water purification with diamond-generated hydroxyl radicals in aqueous solution and oxidant

synthesis, e.g. chlorine/hypochlorite, ozone and peroxodisulphate, and biosensors for pathogen detection and electrochemical analysis.

4.1 Robust, wear-resistant conductive AFM probes

Conductive BD-UNCD AFM probes exploit two important properties of the material: its low wear rate (due to hardness, reduced coefficient of friction, and low chemical reactivity), and its electrochemical properties (low reactivity and wide electrochemical potential window). We have developed both “all-diamond” probes and diamond coated probes, i.e., the structural material of the probes is silicon but it is coated with a thin layer of BD-UNCD.

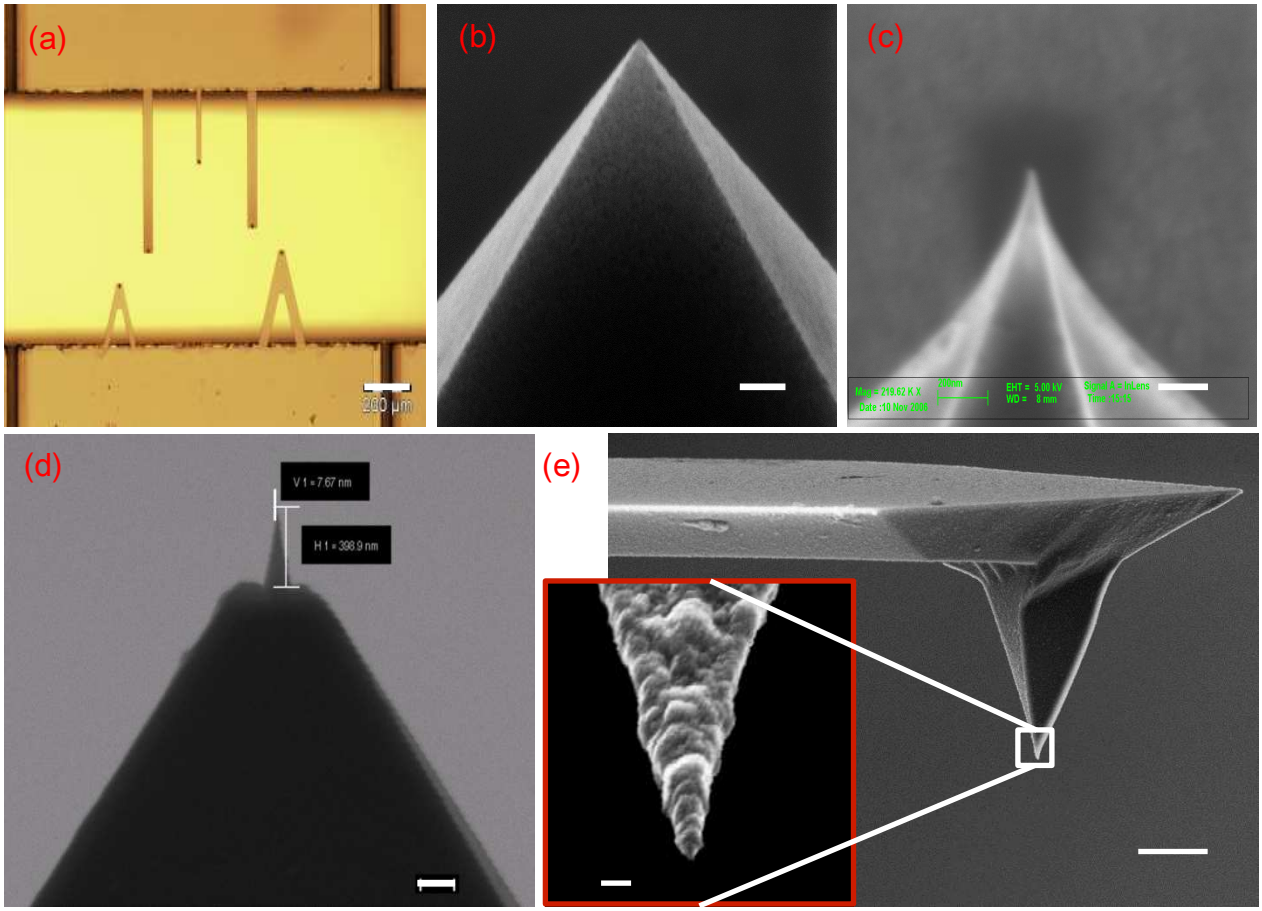

Fig.7 (a) optical micrograph showing monolithic BD-UNCD AFM probes with different cantilever designs, (b) Regular un-sharpened BD-UNCD AFM probes obtained by direct molding into a Si V-groove, (c) BD-UNCD AFM probes obtained by molding into an oxidation-sharpened Si V-groove, (d) BD-UNCD AFM probe tip with FIB-machined spike and (e) BD-UNCD coated Si AFM probe with the tip magnified in insert. Scale bar in (a) represents 200 μm, (b)-(c) represent 100 nm, (d) represents 200 nm, (e) represents 5 μm and insert of (e) represents 100 nm.

The "all-diamond" probes shown in Fig. 7a, with tips and cantilevers are all made from BD-UNCD using a molding technique that involves forming the tip by depositing the diamond onto Si wafers with V-groove pits etched into them, then dissolving the Si. [48-49] Since the grain size for BD-UNCD is smaller than other types of boron doped diamond, BD-UNCD is able to fill the tip molds very accurately and continuously, and the curvature of the released cantilevers of the probes can be close to zero due to precise stress control during the BD-UNCD deposition. The resulting probes' typical tip radii can be as small as 20-50 nm (Fig. 7b). A cross-comparison of wear properties of different AFM probes, including doped and undoped UNCD probes showed no significant differences between the investigated diamond probes. [30] Additional sharpening to achieve tip radii below 10 nm and aspect-ratio

improvements have been demonstrated by oxidation-sharpening the Si molding pits (Fig. 7c) or by additional focused ion beam machining of spikes on the tips (Fig.7d). The value of hardness in BD-UNCD AFM probes is particularly useful in techniques such as scanning spreading resistance microscopy (SSRM) where the conductive tips need to press through native oxides on conductive surfaces, to achieve electrical contact with the samples. Special tip shapes have been developed for such applications, based on molding in V-grooves etched in Si (311) wafers. [30] The electrochemical properties of BD-UNCD are of particular value in probes for scanning electrochemical microscopy (SECM), for which special probes have been developed, with complete electrical SiO_2 insulation excepting a small portion of the tip apex.

BD-UNCD can also be used to coat commercial silicon probes, to confer on them some of the low-wear and conductive properties of the diamond material. Since coating a tip with a film generally increases the tip radius with the thickness of the film, super thin continuous BD-UNCD films were developed for this application. Such probes are of significantly lower cost and have wider design flexibility than "All-diamond" probes, allowing the transformation of any Si probe into a diamond probe by coating. Because of the extremely small grain size of BD-UNCD, the batch fabrication process produces BD-UNCD probes with diameters as small as 30 nm, with average diameters 70 nm across the entire wafer (Fig. 7e). It is noted that, if a NCD film is coated on an AFM probe, even though the initial grain size is as small as 10-20 nm, its facets would tend to form many "spikes" on the top of the probes, leading to "multi-tip effect". [50] Another particular phenomena is that the NCD grain size increases much faster on apex locations or any other sharp structures than those on flat or blunted structures, while BD-UNCD maintains almost the same grain size on different textures. Individually coated AFM probes have been characterized showing tip diameters down to ~20 nm by using a specific tip shape reconstruction method [51]. Wear tests were performed on hard surfaces including quartz, silicon carbide, or UNCD. In one extreme case, the coated probes were scanned for > 1 m at a scan speed of 25 μms^{-1} at temperatures in range of 25-400 °C under loads up to 200 nN. Under these conditions, silicon tips are mostly or completely destroyed, while the UNCD tips exhibit much less or no wear. [52] Another case study of the AFM image evolution of the coated probes involved scanning on a rough MCD diamond surface under contact mode. After > 200 times scanning a 5 μm x 5 μm surface, no change in image quality was observed. By contrast, when Si or SiN probes were tested with the same conditions, the image quality degraded quickly from one scan to another. BD-

UNCD coated Si probes can also be used for low-cost SSRM. If a Si probe is coated with a thick BD-UNCD, a sharp diamond spike can be shaped on the tip by the aforementioned focused ion beam machining method, saving cost by avoiding an "all-diamond" probe manufacturing process.

4.2 Electrochemically durable electrodes

BD-UNCD has been proven to be a durable high-current density electrode material. Compared with their MCD counterparts, BD-UNCD's faster deposition rate provides a decreased cost for these expensive industrial electrodes such as those used for water treatment. Like other types of diamond, it has been proven that the integration of BD-UNCD on Nb, Si, Ta, and W is exceptionally robust [53] due to the strength of the chemical bonds between these substrates and their carbides, the stability of their carbides and the relatively low difference in thermal expansion coefficients. In addition, it was observed that film stress for BD-UNCD can be adjusted and its nanometer size grain can conformably fill the micro- or nano-scale structures of a substrate, which significantly reduces film delamination rate and coating defects such as pin-holes, [54] and therefore the underlying structural materials (metals or silicon) can be protected from the electrochemical attack and thus the electrodes lifetime is increased especially under high current density conditions.

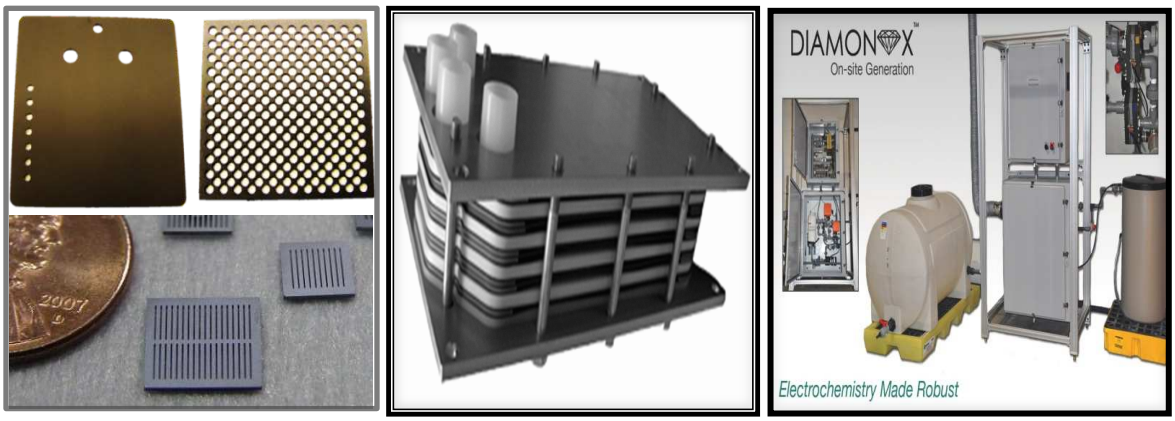

Fig. 8 (a) BD-UNCD electrodes with different geometries and substrates, b) an OSG cell with BD-UNCD electrodes and c) an OSG system with BD-UNCD electrodes.

The authors have developed BD-UNCD based electrodes for use within electrochemical cells and systems, as shown in Fig. 8a, with extremely strong adhesion and electrochemical stability even at extreme voltages/current densities in aqueous solutions. A few different types of accelerated lifetime tests for these electrodes have been conducted on these new

electrodes. In the most aggressive Electrochemical Advanced Oxidation Process (EAOP) protocol, the electrodes were tested up to 4000 A-hr/cm^2 in 1M $NaClO_4$ (i.e. more than 1200 hours under test), with a current density of 2500 mA/cm^2 applied in galvanostatic mode (i.e. 25A for a 10 cm^2 active area electrode). The end of life of the electrodes was determined by both delamination of the anode material from its substrate and an increase in the cell voltage by greater than 3V. In contrast, commercial Dimensionally Stable Anodes (DSA) or graphite electrodes would only survive a few hours (at best) under such conditions as they are typically operated for commercial chlorine (hypochlorite) production at a current density of 100-150 mA/cm^2 or less. In another harsh protocol for the of On-Site Generation (OSG) of oxidants, the electrodes have been tested for more than 4000 A-hr/cm^2 in 1 M solar salt with an applied current density of 2500 mA/ cm^2 in galvanostatic mode and more than 15000 hours in 2M solar salt with an applied current density of 450 mA/ cm^2 without failure or any observed performance degradation. The BD-UNCD coated electrodes are now being applied widely on the (OSG) for chlorine (hypochlorite) (Fig. 8b-c), peroxodisulfate, and peroxodicarbonate, EAOP of wastewater, and ozone generation and wastewater treatment.

4.3 Reliable and highly versatile sensors

Advanced microsensors that can reliably detect target analytes in minimally prepared complex samples in real-time represent one of the greatest challenges for remote environmental monitoring, point-of-use diagnostics, personalized medicine and national security. The two principle issues in integrated electrochemical microsensor development are the achievement of highly stable active bio interfaces that interact with and measured analytes of interest, and the engineering of highly robust transducer electrode materials. This second issue is even more challenging when the sensor also fulfills the desired objectives of being ultra-small in size, versatile in immobilizing a wide range of bio layers, uses simple chemistries in functionalizing biomolecules, promotes long-term functional stability of bio layers, and is amenable to scale-up and large volume manufacturing. BD-UNCD is one of the most promising electrode materials because of its superior electrochemical properties as compared to noble metals and sp^2 hybridized carbon materials [55]. The electrochemical properties of diamond electrodes were found to be sensitive to the surface termination (-H *vs.* -O), allowing further optimization of electronic properties of these electrodes. [56] The diamond surface termination can be readily modified by chemical treatment in hot concentrated H_2SO_4 for an O-terminated surface and with H_2 plasma treatment for a fully H-terminated surface. Diamond microelectrode arrays (MEAs, Fig. 9a) are gaining attention for

biological and chemical sensing because of their high sensitivity and selectivity, multiplexing capability and low cost. [57-60] Electrochemical characterization studies of BD-UNCD demonstrated minimal variation in current peak separation in cyclic voltammograms from the array (<5%), demonstrating highly uniform, reliable microelectrodes with excellent electrochemical behavior: a quasi-reversible electrode process (the separation between oxidation and reduction peaks, ΔE_p~110 mV) (Fig. 9b); two-Q (Constant Phase Element, CPE) behavior; high S/N ratios of greater than 300 and minimal surface oxidation. The MEAs were successfully employed to detect a wide range of analytes including bacteria, [60] dopamine, [61] hormones and heavy metals (Fig.9c-d). BD-UNCD microsensors in microwire geometry (Fig.9e) are more suitable for *in vivo* voltammetry measurement of neuro active substances. These microwire sensors have been tested by using flow injection

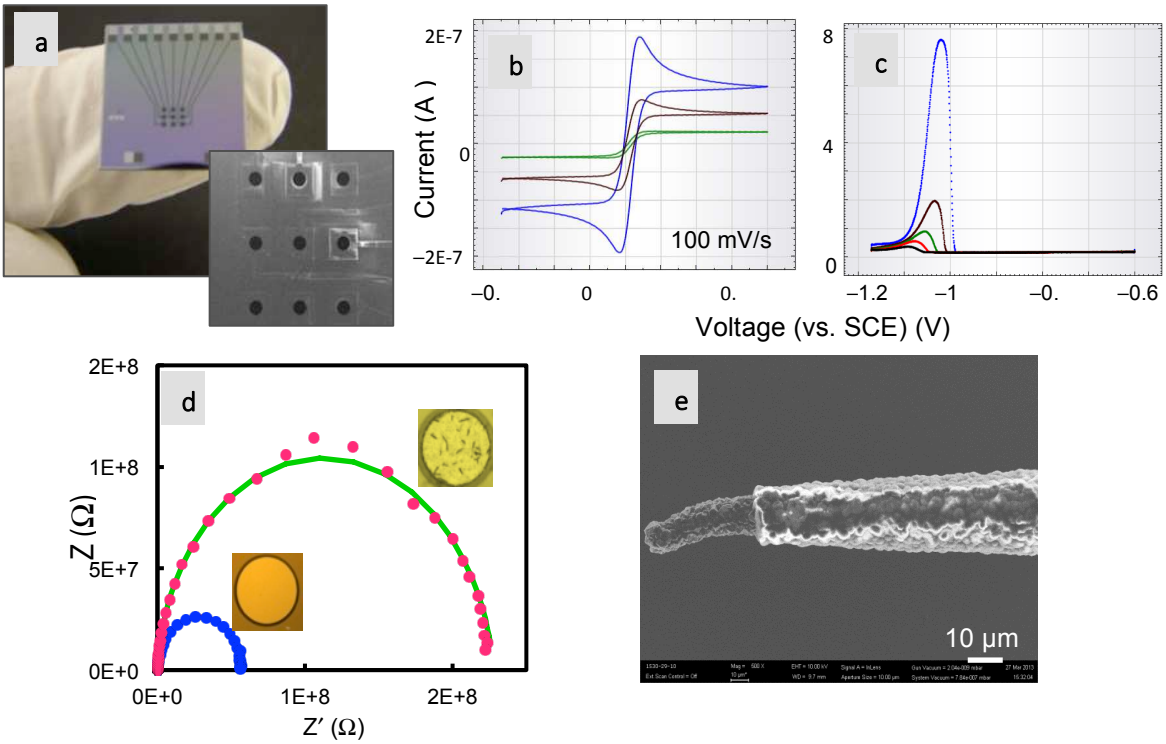

Fig.9. Biological and chemical sensing applications of UNCD 3×3 microarrays. (a) Optical image of microarray. The inset is the SEM image of microarray showing the nine individually addressable microelectrodes of 200 µm diameters. (b) Overlay of the cyclic voltammograms of the 10 µm (green), 50 µm (brown) and 100 µm (blue) microarrays. The electrolyte is 5 mM $Fe(CN)_6^{3-/4-}$ in 1M KCl. (c) Square wave voltammograms of 10 ppm lead on a 100 µm microelectrode after five different deposition times of 0, 5, 25, 55 and 110s (black to blue curves) at –1.52 V vs. Pt reference/counter. (d) Nyquist plot (dotted curve-experimental and solid curve-fitted) of 200 µm microelectrodes modified with anti-K12 bacteria antibody and casein blocker (blue solid circles) and after K12 bacteria capture (pink solid circles). The optical (inset) images of a clean and E. coli K12 captured microelectrodes. The electrolyte used is 5 mM $Fe(CN)_6^{3-/4-}$ in 0.01 M PBS buffer. (e) UNCD coated pre-sharpened tungsten microwire microsensor. The microelectrode is exposed at the tip by insulating with a 3 µm thick parylene and laser etched.

analysis and in rat brains for dopamine detection. Detection limits down to 27 nM were achieved. It is notable that due to the unique properties of the UNCD interface such as its chemical stability, ultra-smooth surface morphology and minimal nonspecific binding, this new electrochemically robust material could emerge as the next best electrochemical transducer for advanced sensing, particularly in implant applications.

5. Conclusions

We have demonstrated boron doped UNCD fabricated with an H-rich/Ar-free and high CH_4/H_2 ratio gas chemistry in a HFCVD reactor. The BD-UNCD fabrication technique is different from both H-rich but low CH_4/H_2 ratio gas chemistry used in conventional NCD/MCD fabrication, and Ar-rich and low CH_4/Ar ratio gas chemistry used in the conventional UNCD fabrication in PECVD tools. Low resistivity down to 0.01 ohm·cm measured by 4-point probe, a uniform and small grain size of 5-15 nm as measured by SEM/TEM, a low roughness down to several nm as measured by AFM, and a high purity sp3 content confirmed by NEXAFS show that the diamond reported here is a heavily boron doped UNCD of high purity. These measurements also revealed feature roughness, nano-texture, grain information, and surface chemistry of BD-UNCD. The results indicate that high purity UNCD is not necessarily linked to low CH_4 content and/or Ar-rich gas, and for the first time BD-UNCD has been fabricated in a HFCVD tool mixed with a boron/methane ratio up to 12500 ppm. Applications of this type of BD-UNCD on conductive AFM probes, robust electrodes and high performance/biocompatible sensors have been demonstrated. An overall hypothesis for the deposition of BD-UNCD in both HFCVD Ar-free and PECVD Ar-rich deposition conditions arises from the results presented, i.e., that a high renucleation rate and the minimization of non-diamond carbon build-up tends to lead to the formation of UNCD. However, this hypothesis will require further investigation and quantification.

Acknowledgement: The work was partially supported by the Defense Threat Reduction Agency under grant HDTRA109C0007, the National Science Foundation SBIR under grant 1058505, the Army Research Office STTR under grant W911NF-12-0102 and the National Institute of Health under grant 2R44HL108534-02. R.W.C. acknowledges support from the National Science Foundation under Grants DMR-1107642, CMMI-1200019, and support from AFOSR under Contract No. FA2386-11-1-4105 AOARD. F.M. acknowledges support from the Marie Curie International Outgoing Fellowship for 161605-4 Career Development within the 7th European Community Framework Program under Contract No. PIOF-GA-

2012-328776. AFM and SEM were conducted by facilities at the Center for Nanoscale Materials at Argonne National Lab. Use of the Nanocharacterization Facility at the University of Pennsylvania is also acknowledged. The authors thank Grace Catausan, Keith Gantz, Charles West, Sabitha Jose and Matthew Hart for diamond synthesis and data collection.

References

1. D. M. Gruen, S. Liu, A. R. Krauss, J. Luo, and X Pan, Fullerenes as precursors for diamond film growth without hydrogen or oxygen additions, Appl. Phys. Lett. 1994, 64, 1502-1504.
2. S. Jiao, A. Sumant, M. A. Kirk, D. M. Gruen, A. R. Krauss, and O. Auciello, Microstructure of ultrananocrystalline diamond films grown by microwave Ar–CH4 plasma chemical vapor deposition with or without added H2, JOURNAL OF APPLIED PHYSICS 2001, 90, 118-122.
3. A. R. Krauss, O. Auciello, M.Q. Ding, D. M. Gruen, Y.Huang, V. V. Zhironv, et al, Electron field emission for ultrananocrystalline diamond films, JOURNAL OF APPLIED PHYSICS 2001, 89, 2958-2967.
4. D. M. Gruen, NANOCRYSTALLINE DIAMOND FILMS, Annu. Rev. Mater. Sci. 1999, 29, 211-259.
5. O. Auciello, Are diamonds a MEMS' best friend? IEEE Microwave Magazine 2007, December, 61-75.
6. D. M. Gruen, S. Liu, A. R. Krauss, and X. Pan, Buckyball microwave plasmas: Fragmentation and diamond-film growth, J. Appl. Phys. 1994, 75, 1758-1763.
7. J. Philip, P. Hessa, T. Feygelson, J. E. Butler, S. Chattopadhyay, K. H. Chen, and L. C. Chen, Elastic, mechanical, and thermal properties of nanocrystalline diamond films, JOURNAL OF APPLIED PHYSICS 2003, 93, 2164-2171.
8. M. N. R. Ashfold, P. W. May, C. A. Rego, N. M. Everitt, Thin Film Diamond by Chemical Vapour Deposition Methods, CHEMICAL SOCIETY REVIEWS 1994, 23, 21-30.
9. Q. Chen, D. M. Gruen, A. R. Krauss, T. D. Corrigan, M. Witek, and G. M. Swain, Journal of The Electrochemical Society 2001, 148, E44-51.
10. P. L. Hagans, P. M. Natishan, B. R. Stoner, and W. E. O'Gradya, Electrochemical Oxidation of Phenol Using Boron-Doped Diamond Electrodes, Journal of The Electrochemical Society 2001, 148, E298-E301.

11. G. M. Swain, R. Ramesham, The Electrochemical Activity of Boron-Doped Polycrystalline Diamond Thin Film Electrodes, Anal. Chem. 1993, 65, 345-351.
12. M. A. Rodrigo, P. A. Michaud, I. Duo, M. Panizza, G. Cerisola and Ch. Comninellis, Electrode for Wastewater Treatment Oxidation of 4-Chlorophenol at Boron-Doped Diamond, J. Electrochem. Soc. 2001, 148, D60-D64.
13. A. Angela, A. Urtiaga, and I. Ortiz, Pilot Scale Performance of the Electro-Oxidation of Landfill Leachate at Boron-Doped Diamond Anodes, Environ. Sci. Technol. 2009, 43, 2035-2040.
14. T.N. Rao, A. Fujishima, Recent advances in electrochemistry of diamond, Diamond and Related Materials 2000, 9, 384-389.
15. J. A. Carlisle, Diamond Films Precious biosensors, Science 2004, 3, 668-669.
16. E. Majid, K. B. Male, J. H. T. Luong, Boron doped diamond biosensor for detection of Escherchia coli, Journal of Agricultural and Food Chemistry 2008, 56, 7691-7695.
17. K. Okano, H. Naruki, Y. Akiba, T Kurosu, M. Lida, and Y. Hirose, Synthesis of Diamond Thin Films Having Semiconductive properties, Japanese Journal of Applied Physics 1988, 27, L173-175.
18. B. Bhushan, V. V. Subramaniam, A. Malshe, B. K. Gupta, and J. Ruan, Tribological properties of polished diamond films, J. Appl. Phys. 1993, 74, 4174-4180.
19. A. R. Konicek, D. S. Grierson, P. U. P. A. Gilbert, W. G. Sawyer, A.V. Sumant, and R.W. Carpick, Origin of Ultralow Friction and Wear in Ultrananocrystalline Diamond 2008, 100, 235502-1-4.
20. A. Sumant, D. S. Grierson, J. E. Gerbi, J. Birrell, U.D. Lanke, O. Auciello, et al., Toward the Ultimate Tribologiecal Interface: surface Chemistry and Nanotribology of Ultrananocrystalline Diamond, Adv. Mater. 2005, 17, 1039-1045.
21. L. Tang, C. Tsai, W.W. Gerberich, L. Kruckeberg and D.R. Kania, Biocompatibility of chemical-vapour-deposited diamond, Biomaterials 1995, 16, 483-488.
22. H. Zeng, P. U. Arumugam and J. A. Carlisle, UltraNanoCrystalline diamond as a biocompatible interfacial material for implantable devices, European Materials Research Society Spring Conference, Lille, France, European Materials Research Society, 2014, In press.
23. S. Bhattacharyya, O. Auciello, J. Birrell, J. A. Carlisle, L.A Crutiss, A.N.Goyette, et al., Synthesis and characterization of highly-conducting nitrogen-doped ultrananocrystalline diamond films, APPLIED PHYSICS LETTERS 2001, 79, 1441-1443.

24. J. Birrell, J. A. Carlisle, O. Auciello, D. M. Gruen, and J. M. Gibson, Morphology and electronic structure in nitrogen-doped ultrananocrystalline diamond, Appl. Phys. Lett. 2002, 81, 2235-2237.
25. Y. Show, M. A. Witek, P. Sonthalia, and G. M. Swain, Characterization and Electrochemical Responsiveness of Boron-Doped Nanocrystalline Diamond Thin-Film Electrodes, Chem. Mater. 2003, 15, 879-888.
26. N. L. Privorotskaya, H. Zeng, J. A. Carlisle, R. Bashir, and William P. King, Piezoresistive Microcantilevers From Ultrananocrystalline Diamond, JMEMS 2010, 19, 1234-1242
27. J. E. Butler and A. V. Sumant, The CVD of Nanodiamond Materials, Chem. Vap. Deposition 2008, 14, 145-160.
28. J. A. Carlisle, C. F. West, and J. W. Zimmer, Diamond film deposition, US Patent Application Publication, US 2009/0017258 A1, 2009
29. H. Liu and D. S. Dandy, Studies on nucleation process in diamond CVD: an overview of recent developments, Diamond and Related Materials, 1995, 4, 1173-1188
30. N. Moldovan, Z. Dai, H. Zeng, J. A. Carlisle, T. D. B. Jacobs, V. Vahdat, *et al*., Advances in Manufacturing of Molded Tips for Scanning Probe Microscopy, JMEMS 2012, 21, 431-445.
31. A. V. Sumant, P.U.P.A. Gilbert, D. S. Griesron, A.R.Konicek, M.Abrecht, J.E.Butler, et al., Surface composition, bonding, and morphology in the nucleation and growth of ultra-thin, high quality nanocrystalline diamond films, Diamond and Related Materials 2007, 16, 718-724.
32. W. Gajewski, P. Achatz, O.A. Williams, K. Haenen, E. Bustarret, M. Stutzmann and J.A. Garrido, Electronic and optical properties of boron-doped nanocrystalline diamond films, Phys. Rev. B 2009, 79, 045206-1-14.
33. S. Bhattacharyya, Mechanism of high n-type conduction in nitrogen-doped nanocrystalline diamond, PHYSICAL REVIEW B 2004, 70, 125412
34. H. Zeng, P. U. Arumugam, S. Siddiqui, and J. A. Carlisle, Low temperature boron doped diamond, Appl. Phys. Lett. 2013, 102, 223108-1-5.
35. J. Birrell, J.E. Gerbi, O. Auciello, J.M. Gibson, J. Johnson, J.A. Carlisle, Interpretation of the Raman spectra of ultrananocrystalline diamond, Diamond & Related Materials 2005, 14, 86-92.
36. A. M. Zaitsev Optical Properties of Diamond- A Hand Book, Springer-Verlag Berlin Heidelberg New York, 2003, 89-102.

37. S. Prawer, K.W. Nugent, D.N. Jamieson, J.O. Orwa, L.A. Bursill, J.L. Peng, The Raman spectrum of nanocrystalline diamond, Chemical Physics Letters 2000, 332, 93-97.
38. A. C. Ferrari and J. Robertson, Origin of the 1150-cmÀ1 Raman mode in nanocrystalline diamond, PHYSICAL REVIEW B 2001, 63, 121405-1-4.
39. R.J. Zhang, S.T. Lee, Y.W. Lam, Characterization of heavily boron-doped diamond films, Diamond and Related Materials 1996, 5, 1288.
40. K. Ushizawa, K. Watanabe, T. Ando, I. Sakaguchi, M. Nishitani-Gamo, Y. Sato, eta al, Boron concentration dependence of Raman spectra on {100} and {111} facets of B-doped CVD diamond, Diamond and Related Materials 1998, 7, 1719-1722.
41. F. Pruvost, E. Bustarret, A. Deneuville, Characteristics of homoepitaxial heavily boron-doped diamond films from their Raman spectra, Diamond and Related Materials 2000, 9, 295-299.
42. Sumant, A.V., Grierson, D.S., Gerbi, J.E., Carlisle, J.A., Auciello, O. and Carpick, R.W., Surface Chemistry and Bonding Configuration of Ultrananocrystalline Diamond Surfaces and Their Effects on Nanotribological Properties, Phys. Rev. B 2007, 76, 235429-1-11.
43. J. Stohr, NEXAFS Spectroscopy, Springer-Verlag, Berlin, Heidelberg, 1992, 162-210
44. O.A. Williams, M. Daenen, J. D'Haen, K. Haenen, J. Maes, V.V. Moshchalkov, et al., Comparison of the growth and properties of ultrananocrystalline diamond and nanocrystalline diamond, Diamond & Related Materials 2006, 15, 654-658.
45. T. Sharda, M. Umenoc, T. Soga, , T. Jimbob, , Growth of nanocrystalline diamond films by biased enhanced microwave plasma chemical vapor deposition, Diamond and Related Materials 2001, 10, 1592-1596.
46. A. T. Sowers, B. L. Ward, S. L. English, and R. J. Nemanicha, Field emission properties of nitrogen-doped diamond films, JOURNAL OF APPLIED PHYSICS VOLUME 1999, 86, 3973-3982.
47. Y. Lifshitz, C. H. Lee, Y. Wu, W. J. Zhang, I. Bello, and S. T. Lee, Role of nucleation in nanodiamond film growth, APPLIED PHYSICS LETTERS 2006, 88, 243114-1-3
48. Agrawal, R.; Moldovan, N.; Espinosa, H. D. An Energy-Based, Model To Predict Wear in Nanocrystalline Diamond Atomic Force Microscopy Tips., J. Appl. Phys. 2009, 106, 064311-1-6.
49. J. Liu, J. K. Notbohm, R. W. Carpick, and K. T. Turner, Method for Characterizing Nanoscale Wear of Atomic Force Microscope Tips, ACSNANO 2010, 4, 3763-3772.

50. Vladimir V. Tsukruk and Srikanth Singamaneni, Scanning Probe Microscopy of Soft Matter: Fundamentals and Practices, Wiley-VCH, 2012, pp 52
51. C. Su, L. Huang, K. Kjoller, K Babcock, Studies of tip wear processes in tapping modeatomic force microscopy, Ultramicroscopy, 2003, 97, 135-144 .
52. P. C. Fletcher, J.R.Felts, Z. Dai, T.D.Jacobs, H. Zeng, W. Lee, et al., Wear-Resistant Diamond Nanoprobe Tips with Integrated Silicon Heater for Tip-Based Nanomanufacturing, ACS NANO 2010, 4, 3338-3344.
53. B. P. Chaplin, I. Wyle, H. Zeng, J. A. Carlisle, J. Farrell, Characterization of the performance and failure mechanisms of boron-doped ultrananocrystalline diamond electrodes, Journal of Applied Electrochemistry 2011, 41, 1329-1340.
54. H. Zeng, P. U. Arumugam and J. A. Carlisle, Ultrananocrystalline diamond as a biocompatible antithrombogenic interfacial material for implantable devices, Physica Status Solidi A: Applications and Materials Science 2014, 31396-1-4
55. R. L. McCreery, Advanced Carbon Electrode Materials for Molecular Electrochemistry, Chem. Rev. 2008, 108, 2646-2687.
56. C.E. Nebel, D. Shin, B. Rezek, N. Tokuda, H. Uetsuka and H. Watanabe, Diamond and biology, J. R. Soc. Interface 2007, 4, 439-461.
57. 49-J. Cvacka, V. Quaiserova, J. Park, Y. Show, A. Muck, and G. M. Swain, Boron-Doped Diamond Microelectrodes for Use in Capillary Electrophoresis with Electrochemical Detection, Anal. Chem. 2003, 75, 2678-2687.
58. A. O. Simm, C. E. Banks, S. Ward-Jones, T. J. Davies, N. S. Lawrence, T. G. J. Jones, et al., Compton, Boron-doped diamond microdisc arrays: electrochemical characterisation and their use as a substrate for the production of microelectrode arrays of diverse metals (Ag, Au, Cu) via electrodeposition, Analyst 2005,130, 1303-1311.
59. Hu, J., Holt, K.B., Foord, J.S. 2009. Focused Ion Beam Fabrication of Boron-Doped Diamond Ultramicroelectrodes. Anal. Chem. 81, 5663–5670.
60. S. Siddiqui, Z. Dai, C. J. Stavis, H. Zeng, N. Moldovana, R. J. Hamers, J. A. Carlisle, P. U. Arumugam, A quantitative study of detection mechanism of a label-free impedance biosensor using ultrananocrystalline diamond microelectrode array, Biosensors and Bioelectronics 2012, 35, 284-290.

61. P. U. Arumugam, H. Zeng, S. Siddiqui, D. P. Covey, J. A. Carlisle, and P. A. Garris, Characterization of ultrananocrystalline diamond microsensors for in vivo dopamine detection, Appl. Phys. Lett. 2013, 102, 253107-1-5.